Geomechanics and Engineering, *Vol. 32, No. 6 (2023) 553-566*
https://doi.org/10.12989/gae.2023.32.6.553

Analysis of circular tank foundation on multi-layered soil subject to combined vertical and lateral loads

Hesham F. Elhuni[1a], Bipin K. Gupta[2b] and Dipanjan Basu*[3]

[1]*Department of Civil and Environmental Engineering, Univ. of Waterloo, Waterloo, ON N2L 3G1, Canada*
[2]*Department of Civil Engineering, IIT Kanpur, Kanpur 208016, UP, India*
[3]*Department of Civil and Environmental Engineering, Univ. of Waterloo, Waterloo, ON N2L 3G1, Canada*

(*Received June 23, 2022, Revised December 23, 2022, Accepted January 9, 2023*)

Abstract. A circular tank foundation resting on the ground and subjected to axisymmetric horizontal and vertical loads and moments is analyzed using the variational principles of mechanics. The circular foundation is assumed to behave as a Kirchhoff plate with in-plane and transverse displacements. The soil beneath the foundation is assumed to be a multi-layered continuum in which the horizontal and vertical displacements are expressed as products of separable functions. The differential equations of plate and soil displacements are obtained by minimizing the total potential energy of the plate-soil system and are solved using the finite element and finite difference methods following an iterative algorithm. Comparisons with the results of equivalent two-dimensional finite element analysis and other researchers establish the accuracy of the method.

Keywords: circular plate; continuum; minimum potential energy; multi-layered soil; soil structure interaction

1. Introduction

Normally, strong winds have been associated with two types of wind in typhoon prone region. The first one is the nature wind and the other one is the typhoon, or say severe tropical cyclone. Many investigations about the vibration and buckling (static stability) characteristics of frames of various types have been carried out. Cheng (2011) have studied the elastic critical loads for plane frames by using the transfer matrix method. A general digital computer method has been described by Cheng and Xu (2012).

Circular tanks are efficient and economic liquid-storage structures because these tanks can save up to 20% volume of construction materials (concrete or steel) compared with rectangular tanks of equal capacities (Jones 1997). These tanks are often placed on the ground (sometimes on top of a granular pad of compacted sand) and are subjected to a combination of vertical and lateral forces arising from self-weight of the tank, weight of stored liquid, internal liquid pressure, temperature variations, and wind (Ghali 2003, Galvis, Smith-Pardo 2020, Useche-Infante *et al*. 2021). The dominating forces are, however, gravity driven (as the heights of these tanks are often low compared with their widths so that wind force is less impactful) because of which these tanks are often designed against axisymmetric gravity loads, consisting of tank self-weight and weight of stored liquid in the vertical direction and internal liquid pressure in radial directions.

*Corresponding author, Professor
E-mail: dipanjan.basu@uwaterloo.ca
[a]Ph.D. Candidate
[b]Assistant Professor

The super-structure part of the tank is typically analyzed as a vertical shell element subjected to radial stresses. Consequently, combinations of axisymmetric horizontal and vertical forces, and moments act on the circular base of the tank and along its edges. The tank base acts as the foundation of the tank and remains in contact with the ground (or granular pad) underneath (Useche-Infante *et al*. 2022). Typically, the tank super-structure (shell and roof loads) generates vertical stresses along the edge of the circular base that are of the order 70 kPa, and the weight of the retained liquid generates vertical stresses over the entire area of the base that are of the order of 400 kPa (Rosenberg and Journeaux 1982). At the same time, the lateral thrust from the liquid generates radially outward axisymmetric horizontal forces along the edge of the base. Thus, the soil mass underneath the tank foundation is subjected to forces and displacements both in the vertical and horizontal directions (Booker and Small 1983).

The serviceability limit states against which tank foundations are designed include total and differential settlements. Differential settlement (the difference between the settlements at the center and the edge of tank foundation) is often detrimental to the structural integrity because of which it is routinely estimated (Marr *et al*. 1982, Ghali 2003, D'orazio and Duncan 1987, Remadna *et al*. 2017). A better representation of the structural distress caused by differential settlement may be obtained by angular distortion (Salgado 2008), which, for symmetrically loaded circular tanks, is the angle formed with the horizontal by the deformed tank foundation between the edge and the center. Maintaining the differential settlement and angular distortion within tolerable limits is very crucial in the design of circular tank foundations. Even a small differential settlement may induce large distortions at the top of the vertical shell (i.e., tank wall), and this can

ISSN: 2005-307X (Print), 2092-6219 (Online)

damage the seal between the shell and the roof, and can generate large bending deformations in the roof (Bell and Wakiri 1980). Limits on angular distortions tolerable by circular tank foundations are available in the literature (Gunerathne *et al*. 2018).

In order to estimate the settlement of circular tank foundations, the tank base is conventionally analyzed as a circular plate resting on a bed of linear elastic Winkler springs characterized by the spring constant ks, which is related to the soil subgrade modulus (Brown 1969, Hemsley 1987, Pavlovic 2001). Studies on response of plates resting on Winkler foundations are available, although circular plates are not extensively studied (Komlev and Makeev 2018, Li *et al*. 2013, Utku *et al*. 2000, Utku and Çıtıpıtıoğlu 2000, Timoshenko and Woinowsky-Krieger 1959). However, the Winkler model does not represent the soil behavior properly because the vertical Winkler springs are assumed to work in isolation with respect to each other as a result of which the resistance of soil arising from shear stresses are neglected. The Winkler model is improved by the addition of a second parameter ts to the model that takes into account the interaction between adjacent springs (Pasternak 1954, Hetenyi 1946, Filonenko-Borodich 1945). Thus, the two-parameter models are more realistic than the Winkler model in capturing the soil behavior because both the compressive and shear resistances of soil are captured through the parameters k_s and t_s. Analysis of circular plates with two-parameter models has been performed as well (Buczkowski and Torbacki 2001, Worku and Habte 2022). However, the difficulty in using the two-parameter models is that the two parameters k_s and t_s cannot be reliably obtained from measurable soil properties and are often inaccurately determined from ad hoc, empirical equations (Bowles 1996).

Ideally, soil should be modeled as a continuum for foundation-related problems to capture the multi-axial stress-strain behavior of soil in response to foundation loading. Vlasov and Leont'ev (1966) modeled the soil beneath circular plates subjected to axisymmetric vertical loads as a simplified continuum with zero horizontal soil displacement and the vertical soil displacement approximated by a product of separable functions. Vallabhan and Das (1991) improved the model of Vlasov and Leont'ev (1966) by reducing the assumptions and by incorporating an iterative solution algorithm, and analyzed circular tank foundations subjected to axisymmetric vertical loads. Gunerathne *et al*. (2018) adopted the model by Vallabhan and Das (1991) and made artificial adjustments to the soil elastic constants to estimate differential settlement underneath circular tank foundations. Later, Gunerathne *et al*. (2019) extended the analysis of Vallabhan and Das (1991) by incorporating multiple soil layers. The advantage of the simplified continuum approach of Vallabhan and Das (1991), Gunerathne *et al*. (2018), and Gunerathne *et al*. (2019) is that solutions are obtained much faster than conventional finite element (FE) analysis, but the limitation is that horizontal displacement in the soil underneath foundation is neglected because of which artificially stiff foundation response is obtained and the effect of horizontal forces acting on the tank foundation cannot be incorporated in the analysis.

The elastic half-space theory has also been used to obtain analytical expressions of settlement under a loaded circular region (representing an infinitely flexible foundation) and a rigid circular foundation (Ahlvin and Ulery 1962, Gerrard and Harrison 1970, Melerski 1991); however, these analytical solutions do not predict accurate foundation response because tank foundations are neither completely rigid nor infinitely flexible. Numerical methods such as the FE and finite difference (FD) methods can be used to analyze circular tank foundations, and has been used sparsely in the literature (Mahmood 1984, Kukerti 1997); but the problem with these numerical analyses is that these are time consuming and are generally not adopted in routine projects.

In this paper, a continuum-based analysis is developed to predict the flexural behavior of circular tank foundations resting on multi-layered elastic soil and subjected to axisymmetric vertical and horizontal forces and moments. The tank base is modeled using the thin plate theory and the soil underneath is modeled as a multi-layered continuum with rationally assumed vertical and horizontal displacement fields. The principle of minimum potential energy and variational calculus are used to obtain the differential equations governing the plate and soil displacements under equilibrium. The differential equations are solved using the FE and FD methods following an iterative algorithm. The analysis produces accurate plate response as verified with equivalent two-dimensional FE analysis. The advantage of the present analysis is that the results produced are much faster than equivalent FE analysis. The present analysis is inspired by the simplified continuum approach of Vallabhan and Das (1991) with the improvement that horizontal soil displacement beneath the circular foundation is not assumed to be zero and is explicitly taken into account. This makes the analysis more accurate which is verified by comparisons with other analysis through multiple examples.

2. Analysis

2.1 Problem definition

A circular plate of diameter B, radius r_p (= B/2), depth (thickness) t_p, Young's modulus E_p, Poisson's ratio υ_p, extensional rigidity C [= $E_p t_p/(1 - \upsilon_p^2)$], and flexural rigidity D [= $E_p t_p^3/\{12(1 - \upsilon_p^2)\}$] is assumed to rest on top of a multi-layered continuum (soil) consisting of n layers (Fig. 1). The i^{th} soil layer extends vertically downward to a depth H_i ($H_0 = 0$) so that the thickness of the i^{th} layer $T_i = H_i - H_{i-1}$.

The total thickness of the n layers is H_{total} ($=\sum_{i=1}^{n} T_i$). The bottom n^{th} layer rests on top of a rigid layer (e.g., bed rock), which means that the displacements at a depth $z = H_n = H_{total}$ are all zero. The plate is always in full contact with the layered continuum during loading. Each foundation layer i is homogeneous, isotropic, and linear elastic with Young's modulus E_{si} and Poisson's ratio υ_{si}.

A set of static axisymmetric loads (Fig. 1) act on the plate — a transverse (vertical) line load Q (kN/m) acts along the perimeter (edge) of the plate, a distributed transverse (vertical) load $q(r)$ (kN/m^2) acts over the entire area of the plate, a line moment M (kN.m/m) acts along the perimeter (edge) of the plate, and a radial (horizontal) load N (kN/m) acts along the perimeter of the plate (the line of action of N lie in the neutral plane of the plate). The combination of Q, q, M, and N produces flexure, transverse shear, and membrane (axial) stresses in the plate.

A right-handed cylindrical (r-θ-z) coordinate system is assumed for analysis and is attached to the center of the circular plate with r positive radially outward, z positive vertically downward, and θ positive in the counter-clockwise direction when looked down from the top. As the soil (continuum) beneath the plate deforms beyond the loaded circular region of the plate, it is necessary to consider a soil domain in the radial direction extending beyond the edges of the circular plate (Fig. 1). Accordingly, the analysis domain in the continuum is extended to a radial distance βr_p from the center of the plate beyond the edge of the plate and this eliminated any boundary effects (the dimensionless factor $\beta > 1$ and its actual value is determined by trial and error for a given problem). Thus, a cylindrical soil domain of radius βr_p and depth H_{total} is assumed in the analysis.

2.2 Soil displacements, strains, stresses, and potential energy

For the axisymmetric problem considered, the radial (horizontal) soil displacement u_r and the vertical soil displacement u_z are expressed as products of separable functions (see Fig. 1)

$$u_r = u(r)\psi(z) \tag{1a}$$

$$u_z = w(r)\phi(z) \tag{1b}$$

where $w(r)$ and $u(r)$ are the vertical and radial (horizontal) displacements at the top surface of the continuum, which are the same as the transverse and radial (horizontal) displacements of the plate for $-r_p \le r \le r_p$, and $\phi(z)$ and $\psi(z)$ are dimensionless displacement functions varying with depth. It is assumed in the analysis that $\phi(0) = \psi(0) = 1$, which ensures perfect contact between the plate and the underlying continuum, and that $\phi(H_{\text{total}}) = \psi(H_{\text{total}}) = 0$, which ensures that the vertical and horizontal displacements in the continuum, arising from applied forces on the tank, decrease with an increase in depth and become zero at the interface with the rigid layer.

For the displacement field described in Eq. (1), the strain tensor at any point in the continuum (soil) is given by

$$\varepsilon_{ij} = \begin{Bmatrix} \varepsilon_{rr} \\ \varepsilon_{zz} \\ \varepsilon_{\theta\theta} \\ \gamma_{rz} \end{Bmatrix} = \begin{Bmatrix} \dfrac{du_r}{dr} \\ \dfrac{du_z}{dz} \\ \dfrac{u_r}{r} \\ \dfrac{du_r}{dz} + \dfrac{du_z}{dr} \end{Bmatrix} = \begin{Bmatrix} \dfrac{du}{dr}\psi \\ \dfrac{d\phi}{dz}w \\ \dfrac{u\psi}{r} \\ \dfrac{d\psi}{dz}u + \dfrac{dw}{dr}\phi \end{Bmatrix} \tag{2}$$

The elastic constitutive relationship relates the strain tensor at any point within the continuum to the corresponding stress tensor (see Fig. 1)

$$\begin{aligned} \sigma_{ij} = \begin{Bmatrix} \sigma_{rr} \\ \sigma_{zz} \\ \sigma_{\theta\theta} \\ \tau_{rz} \end{Bmatrix} &= \frac{E_s(1-\upsilon_s)}{(1+\upsilon_s)(1-2\upsilon_s)} \\ &\times \begin{bmatrix} 1 & \dfrac{\upsilon_s}{(1-\upsilon_s)} & \dfrac{\upsilon_s}{(1-\upsilon_s)} & 0 \\ \dfrac{\upsilon_s}{(1-\upsilon_s)} & 1 & \dfrac{\upsilon_s}{(1-\upsilon_s)} & 0 \\ \dfrac{\upsilon_s}{(1-\upsilon_s)} & \dfrac{\upsilon_s}{(1-\upsilon_s)} & 1 & 0 \\ 0 & 0 & 0 & \dfrac{(1-2\upsilon_s)}{\left[2(1-\upsilon_s)\right]} \end{bmatrix} \\ &\times \begin{Bmatrix} \dfrac{du}{dr}\psi \\ \dfrac{d\phi}{dz}w \\ \dfrac{u\psi}{r} \\ \dfrac{d\psi}{dz}u + \dfrac{dw}{dr}\phi \end{Bmatrix} \end{aligned} \tag{3}$$

The stresses and strains can be used to calculate the strain energy density $U_{D\text{-soil}}$ within any soil layer i as

$$\begin{aligned} U_{D-\text{soil}} &= \frac{1}{2}\sigma_{jk}\varepsilon_{jk} = \frac{1}{2}\left[\sigma_{rr}\varepsilon_{rr} + \sigma_{zz}\varepsilon_{zz} + \sigma_{\theta\theta}\varepsilon_{\theta\theta} + \tau_{rz}\gamma_{rz}\right] \\ &= \frac{1}{2}\Bigg[\bar{E}_{si}\left(\psi_i^2\left(\frac{du}{dr}\right)^2 + w^2\left(\frac{d\phi_i}{dz}\right)^2 + \frac{\psi_i^2 u^2}{r^2}\right) \\ &\quad + 2\bar{E}_{si}\left(\frac{\upsilon_{si}}{1-\upsilon_{si}}\right)\left(\frac{du}{dr}\frac{\psi_i^2 u}{r} + \frac{du}{dr}\frac{d\phi_i}{dz}\psi_i w + \frac{d\phi_i}{dz}\frac{\psi_i wu}{r}\right) \\ &\quad + G_{si}\left(\frac{dw}{dx}\phi_i + \frac{d\psi_i}{dz}u\right)^2\Bigg] \end{aligned} \tag{4}$$

where ϕ_i and ψ_i represent the functions $\phi(z)$ and $\psi(z)$ within the i^{th} layer, and $\bar{E}_{si}$ (constrained modulus) and G_{si} (shear modulus) are given by

$$\bar{E}_{si} = \frac{E_{si}(1-\upsilon_{si})}{(1+\upsilon_{si})(1-2\upsilon_{si})} \tag{5a}$$

$$G_{si} = \frac{E_{si}}{2(1+\upsilon_{si})} \tag{5b}$$

The total potential energy Π_{soil} of the soil is obtained by integrating the strain energy density over the entire soil volume Ω_{soil} participating in the deformation as

$$\begin{aligned} \Pi_{\text{soil}} &= \int_{\Omega} U_{D-\text{soil}}\, d\Omega_{\text{soil}} \\ &= \sum_{i=1}^{n}\frac{1}{2}\int_{H_{i-1}}^{H_i}\int_0^{2\pi}\int_0^{r_p 2\beta}\Bigg[\bar{E}_{si}\left(\psi_i^2\left(\frac{du}{dr}\right)^2 + w^2\left(\frac{d\phi_i}{dz}\right)^2 + \frac{\psi_i^2 u^2}{r^2}\right) \\ &\quad + 2\bar{E}_{si}\left(\frac{\upsilon_{si}}{1-\upsilon_{si}}\right)\left(\frac{du}{dr}\frac{\psi_i^2 u}{r} + \frac{du}{dr}\frac{d\phi_i}{dz}\psi_i w + \frac{d\phi_i}{dz}\frac{\psi_i wu}{r}\right) \\ &\quad + G_{si}\left(\frac{dw}{dx}\phi_i + \frac{d\psi_i}{dz}u\right)^2\Bigg] r\,dr\,d\theta\,dz \end{aligned} \tag{6}$$

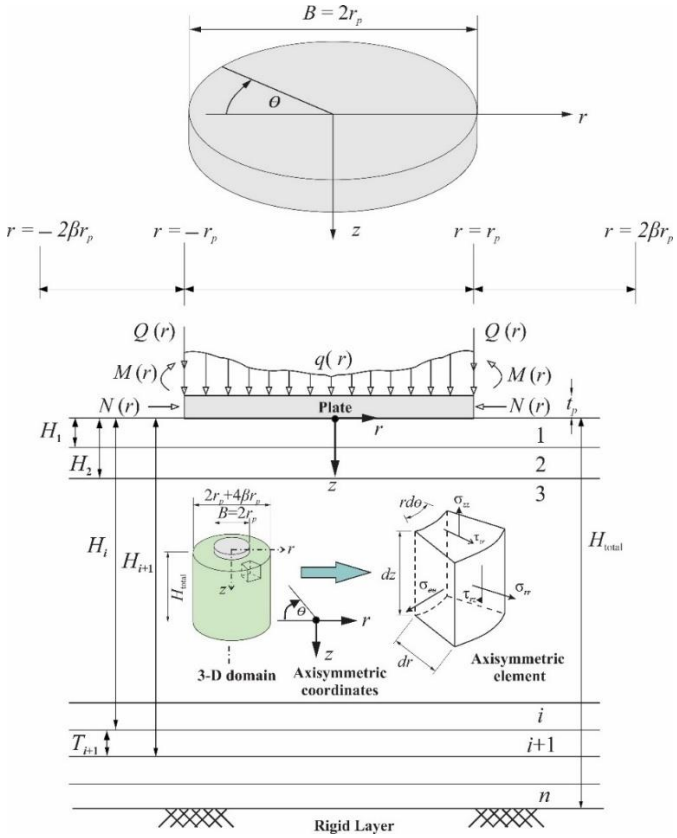

Fig. 1 Plate-soil interaction model

2.3 Plate potential energy

In this study, plate deformation is assumed to follow the Kirchhoff (thin plate) theory of circular plate, according to which a straight line normal to the neutral plane of the plate remains straight and normal to the neutral plane after deformation (Reddy 2006). The potential energy Π_{plate} of a circular plate in polar coordinates, including both extensional and transverse displacements, is given by (Reddy 2006, Chandrasekaran and Kunukkasseril 1976, and Timoshenko 1959)

$$\begin{aligned}\Pi_{\text{plate}} &= \int_{\Omega} U_{D-\text{plate}}\, d\Omega_{\text{plate}} \\ &= \frac{D}{2}\int_0^{2\pi}\int_0^{r_p}\left[\left(\nabla^2 w\right)^2 - \frac{2\left(1-2\upsilon_p\right)}{r}\frac{dw}{dr}\frac{d^2w}{dr^2}\right] r dr d\theta \\ &+ \frac{C}{2}\int_0^{2\pi}\int_0^{r_p}\left[\frac{du}{dr}+\frac{u}{r}\right]^2 r dr d\theta\end{aligned} \tag{7}$$

where $U_{D\text{-plate}}$ is the strain energy density of the plate considering both extensional and transverse displacements over the domain Ω_{plate}, and $\nabla^2 = \left[\left(d^2/dr^2\right)+\left(1/r\right)\left(d/dr\right)\right]$

2.4 Principle of minimum potential energy

The principle of minimum potential energy is used to obtain the differential equations governing the equilibrium of the plate and soil under static loads

$$\delta\Pi_{\text{system}} = \delta\left(\Pi_{\text{soil}} + \Pi_{\text{plate}} + \Pi_{\text{load}}\right) = 0 \tag{8}$$

where δ is the variational operator, Π_{system} is the total potential energy of the plate-soil system, and Π_{load} is the external work done by the non-conservative forces acting on the system, given by

$$\begin{aligned}\Pi_{\text{load}} = &-\int_0^{2\pi}\int_0^{r_p}\left(q(r)\, w\, r dr d\theta\right) - \int_0^{2\pi} N u\big|_{r=r_p} r d\theta \\ &- \int_0^{2\pi} Q w\big|_{r=r_p} r d\theta + \int_0^{2\pi} M\frac{\partial w}{\partial r}\bigg|_{r=r_p} r d\theta\end{aligned} \tag{9}$$

Substituting Eqs. (6), (7), and (9) in Eq. (8) results in

$$\begin{aligned}\delta\Pi_{\text{system}} = \delta\Bigg[&\frac{D}{2}\int_0^{2\pi}\int_{-r_p}^{r_p}\left\{\left(\nabla^2 w\right)^2 - \frac{2\left(1-2\upsilon_p\right)}{r}\frac{dw}{dr}\frac{d^2w}{dr^2}\right\} r dr d\theta \\ &+ \frac{C}{2}\int_0^{2\pi}\int_{-r_p}^{r_p}\left\{\frac{du}{dr}+\frac{u}{r}\right\}^2 r dr d\theta \\ &+ \int_{-r_p(2\beta+1)}^{r_p(2\beta+1)}\sum_{i=1}^{n}\int_{H_{i-1}}^{H_i}\int_0^{2\pi}\Bigg\{\bar{E}_{si}\left(\psi_i^2\left(\frac{du}{dr}\right)^2 + w^2\left(\frac{d\phi_i}{dz}\right)^2 + \frac{\psi_i^2 u^2}{r^2}\right) \\ &+ \bar{E}_{si}\left(\frac{\upsilon_{si}}{1-\upsilon_{si}}\right)\left(\frac{du}{dr}\frac{\psi_i^2 u}{r} + \frac{du}{dr}\frac{d\phi_i}{dz}\psi_i w + \frac{d\phi_i}{dz}\frac{\psi_i w u}{r}\right) \\ &+ G_{si}\left(\frac{dw}{dx}\phi_i + \frac{d\psi_i}{dz}u\right)^2\Bigg\} r dr d\theta dz \\ &+ \Bigg\{-\int_0^{2\pi}\int_{-r_p}^{r_p}\left(q(r)\, w\, r dr d\theta\right) - \int_0^{2\pi} N u\big|_{r_p} r d\theta \\ &- \int_0^{2\pi} Q w\big|_{r_p} r d\theta + \int_0^{2\pi} M\frac{dw}{dr}\bigg|_{r_p} r d\theta\Bigg\}\Bigg] = 0\end{aligned} \tag{10}$$

Eq. (10) is rearranged as

$$\begin{aligned}\delta\Pi_{\text{system}} = \Bigg[& 2\pi D\int_{-r_p}^{r_p}\left\{r\frac{d^4w}{dr^4}+2\frac{d^3w}{dr^3}+\frac{1}{r}\frac{d^2w}{dr^2}+\frac{1}{r^2}\frac{dw}{dr}\right\}dr\delta w \\ & +2\pi C\int_{-r_p}^{r_p}\left\{\frac{u}{r^2}-r\frac{d^2u}{dr^2}-\frac{du}{dr}\right\}dr\delta u \\ & +2\pi\int_{-r_p(2\beta+1)}^{r_p(2\beta+1)}\left\{(\eta_1-\eta_3)\left(r\frac{du}{dr}+u\right)+\eta_2 rw \right. \\ & \qquad \left. -\eta_4\left(r\frac{d^2w}{dr^2}+\frac{dw}{dr}\right)\right\}dr\delta w \\ & +2\pi\int_{-r_p(2\beta+1)}^{r_p(2\beta+1)}\left\{-(\eta_1-\eta 3)r\frac{dw}{dr}+\left(\frac{\eta_6}{r}+\eta_7 r\right)u \right. \\ & \qquad \left. -\eta_6\frac{du}{dr}-\eta_8 r\frac{d^2u}{dr}\right\}dr\delta u \\ & +\sum_{i=1}^{n}2\pi\int_{H_{i-1}}^{H_i}\{(\xi_1+2\xi_1+\xi_4)\psi_i \\ & +\left\{(\xi_1+2\xi_1+\xi_4)\psi_i+(\xi_3+\xi_5-\xi_7)\frac{d\phi_i}{dz}-\xi_6\frac{d^2\psi_i}{dz^2}\right\}dz\delta\psi \\ & +\sum_{i=1}^{n}2\pi\int_{H_{i-1}}^{H_i}\left\{(\xi_7-\xi_3-\xi_5)\frac{d\psi_i}{dz}+\xi_8\phi_i-\xi_9\frac{d^2\phi_i}{dz^2}\right\}dz\delta\phi \\ & +2\pi D\left\{r\frac{d^2w}{dr^2}+\upsilon_p\frac{dw}{dr}\right\}\Big|_0^{r_p}\delta\left(\frac{dw}{dr}\right) \\ & -2\pi D\left\{r\frac{d^3w}{dr^3}+\frac{d^2w}{dr^2}-\frac{dw}{dr}\right\}\Big|_0^{r_p}\delta w \\ & +2\pi C\left\{\upsilon_p u+r\frac{du}{dr}\right\}\Big|_{-r_p}^{r_p}\delta u \\ & +2\pi\left\{\eta_3 ru+\eta_4 r\frac{dw}{dr}\right\}\Big|_{-r_p(2\beta+1)}^{r_p(2\beta+1)}\delta w \\ & +2\pi\left\{\eta_6 r\frac{du}{dr}+\eta_8 u+\eta_1 rw\right\}\Big|_{-r_p(2\beta+1)}^{r_p(2\beta+1)}\delta u \\ & +\sum_{i=1}^{n}2\pi\left\{\xi_6\frac{d\psi_i}{dz}+\xi_7\phi_i\right\}\Big|_{H_{i-1}}^{H_i}\delta\psi+ \\ & +\sum_{i=1}^{n}2\pi\left\{(\xi_3+\xi_5)\psi_i+\xi_9\frac{d\phi_i}{dz}\right\}\Big|_{H_{i-1}}^{H_i}\delta\phi \\ & -\left\{2\pi\int_0^{r_p}q(r)rdr-2\pi rQ\big|_{r=r_p}\right\}\delta w \\ & -\left\{2\pi rN\big|_{r=r_p}\right\}\delta u-\left\{2\pi rM\big|_{r=r_p}\right\}\delta\left(\frac{dw}{dr}\right)\Bigg]=0 \end{aligned} \tag{11}$$

where

$$\eta_1=\sum_{i=1}^{n}\int_{H_{i-1}}^{H_i}\overline{E}_{si}\left(\frac{\upsilon_{si}}{1-\upsilon_{si}}\right)\frac{d\phi_i}{dz}\psi_i dz \quad ,$$

$$\eta_2=k_s=\sum_{i=1}^{n}\int_{H_{i-1}}^{H_i}\overline{E}_{si}\left(\frac{d\phi_i}{dz}\right)^2 dz \ , \ \eta_3=\sum_{i=1}^{n}\int_{H_{i-1}}^{H_i}G_{si}\phi_i\frac{d\psi_i}{dz}dz \ ,$$

$$\eta_4=2t_s=\sum_{i=1}^{n}\int_{H_{i-1}}^{H_i}G_{si}\phi_i^2 dz \ , \ \eta_5=\sum_{i=1}^{n}\int_{H_{i-1}}^{H_i}\overline{E}_{si}\left(\frac{\upsilon_{si}}{1-\upsilon_{si}}\right)\psi_i^2 dz \ ,$$

$$\eta_6=\sum_{i=1}^{n}\int_{H_{i-1}}^{H_i}\overline{E}_{si}\ \psi_i^2 dz \ , \ \eta_7=\sum_{i=1}^{n}\int_{H_{i-1}}^{H_i}G_{si}\left(\frac{d\psi_i}{dz}\right)^2 dz \ ,$$

$$\eta_8=\sum_{i=1}^{n}\int_{H_{i-1}}^{H_i}\overline{E}_{si}\left(\frac{\upsilon_{si}}{1-\upsilon_{si}}\right)\psi_i^2 dz \ , \ \xi_1=\int_{-r_p(2\beta+1)}^{r_p(2\beta+1)}\overline{E}_{si}\left(\frac{du}{dr}\right)^2 rdr \ ,$$

$$\xi_2=\int_{-r_p(2\beta+1)}^{r_p(2\beta+1)}\overline{E}_{si}\left(\frac{\upsilon_{si}}{1-\upsilon_{si}}\right)u\frac{du}{dr}dr \ ,$$

$$\xi_3=\int_{-r_p(2\beta+1)}^{r_p(2\beta+1)}\overline{E}_{si}\left(\frac{\upsilon_{si}}{1-\upsilon_{si}}\right)r\frac{du}{dr}w\ dr \ , \ \xi_4=\int_{-r_p(2\beta+1)}^{r_p(2\beta+1)}\overline{E}_{si}\frac{u^2}{r}.dr \ ,$$

$$\xi_5=\int_{-r_p(2\beta+1)}^{r_p(2\beta+1)}\overline{E}_{si}\left(\frac{\upsilon_{si}}{1-\upsilon_{si}}\right)w\ u\ dr \ , \ \xi_6=\int_{-r_p(2\beta+1)}^{r_p(2\beta+1)}G_{si}u^2 r\ dr \ ,$$

$$\xi_7=\int_{-r_p(2\beta+1)}^{r_p(2\beta+1)}G_{si}u\frac{dw}{dr}r\ dr \ , \ \xi_8=\int_{-r_p(2\beta+1)}^{r_p(2\beta+1)}G_{si}\left(\frac{dw}{dr}\right)^2 rdr \ , \text{ and}$$

$$\xi_9=\int_{-r_p(2\beta+1)}^{r_p(2\beta+1)}\overline{E}_{si}w^2 rdr \ .$$

2.5 Differential equations for vertical displacements of plate and soil surface

Considering the variation of function *w* in Eq. (11), the governing differential equations for transverse displacement of the plate and vertical displacement of the soil surface can be obtained along with the corresponding boundary conditions. For the domain $-r_p \le r \le r_p$ (i.e., over the domain within which the plate is present), the governing differential equation of transverse plate displacement is given by

$$D\nabla^4 w-2t_s\nabla^2 w+k_s w+(\eta_1-\eta_3)\nabla u=q(r) \qquad \left(-r_p\le r\le r_p\right) \tag{12a}$$

For the domains $-\beta r_p \le r \le -r_p$ and $r_p \le r \le \beta r_p$ (i.e., over the domain with no plate), the vertical displacement of the top surface of the soil is governed by the following differential equation

$$-2t_s\nabla^2 w+k_s w+(\eta_1-\eta_3)\nabla u=0 \qquad \left(-\beta\ r_p\le r\le -r_p\right) \text{ and } \left(r_p\le r\le \beta\ r_p\right) \tag{12b}$$

In Eqs. (12(a)) and (12(b)), the differential operators are defined as $\nabla=\left(\frac{d}{dr}+\frac{1}{r}\right)$, $\nabla^2=\left(\frac{d^2}{dr^2}+\frac{1}{r}\frac{d}{dr}\right)$, and

$$\nabla^4=\left(\frac{d^4}{dr^4}+\frac{2}{r}\frac{d^3}{dr^3}+\frac{1}{r^2}\frac{d^2}{dr^2}+\frac{1}{r^3}\frac{d}{dr}\right).$$

The boundary conditions associated with the differential Eqs. (12(a)) and (12(b)) are also obtained from Eq. (11). The domain of the problem ($-\beta r_p \le r \le \beta r_p$) is chosen sufficiently large in the radial directions such that the vertical displacement at the outer boundaries of the domain is zero; i.e., $w = 0$ at $r = -\beta r_p$ and $r = \beta r_p$. At the plate edges ($r = -r_p$ and $r = r_p$), the continuity of displacements, and equilibrium in terms of shear force and bending moment is satisfied (the plate edge is assumed to be free to deflect and rotate)

$$w_{\text{Right}}\big|_{r=-r_p}=w_{\text{Left}}\big|_{r=-r_p} \tag{13a}$$

$$w_{\text{Left}}\big|_{r=r_p} = w_{\text{Right}}\big|_{r=r_p} \tag{13b}$$

$$\left[-2t_s\frac{dw}{dr}-\eta_3 ru\right]_{\text{Left}}\Bigg|_{r=-r_p} = \left[D\frac{d}{dr}\left\{\frac{1}{r}\frac{d}{dr}\left(r\frac{dw}{dr}\right)\right\}-2t_s\frac{dw}{dr}-\eta_3 ru-rQ\right]_{\text{Right}}\Bigg|_{r=-r_p} \tag{13c}$$

$$\left[-2t_s\frac{dw}{dr}-\eta_3 ru\right]_{\text{Right}}\Bigg|_{r=r_p} = \left[D\frac{d}{dr}\left\{\frac{1}{r}\frac{d}{dr}\left(r\frac{dw}{dr}\right)\right\}-2t_s\frac{dw}{dr}-\eta_3 ru-rQ\right]_{\text{Left}}\Bigg|_{r=r_p} \tag{13d}$$

$$\left[-D\left(r\frac{d^2w}{dr^2}+\upsilon_p\frac{dw}{dr}\right)+rM\right]\Bigg|_{r=-r_p \text{ and } r=r_p} = 0 \tag{13d}$$

2.6 Differential equations for horizontal displacements of plate and soil surface

Considering the variation of the function u in Eq. (11), the governing differential equations for the radial (horizontal) displacements in the plate-soil system can be obtained along with the corresponding boundary conditions. For the domain $-r_p \le r \le r_p$ (i.e., the radial domain covering the plate), the differential equation governing the horizontal displacement in the plate is given by

$$C\left(\frac{u}{r}-r\nabla^2 u\right)-\eta_8\frac{d^2u}{dr^2}-\eta_6\frac{1}{r}\frac{du}{dr}+\left(\frac{\eta_6}{r^2}+\eta_7\right)u-\left(\eta_1-\eta_3\right)\frac{dw}{dr}=0 \qquad \left(-r_p \le r \le r_p\right) \tag{14a}$$

For the domains $-\beta r_p \le r \le -r_p$ and $r_p \le r \le \beta r_p$ (i.e., over the radial domain with no plate), the radial displacement of the top surface of the soil is governed by the following differential equation

$$-\eta_8\frac{d^2u}{dr^2}-\eta_6\frac{1}{r}\frac{du}{dr}+\left(\frac{\eta_6}{r^2}+\eta_7\right)u-\left(\eta_1-\eta_3\right)\frac{dw}{dr}=0 \qquad \left(-\beta r_p \le r \le -r_p\right) \text{ and } \left(r_p \le r \le \beta r_p\right) \tag{14b}$$

The boundary conditions for Eqs. (14(a)) and (14(b)) are obtained from Eq. (11). As the domain of the problem ($-\beta r_p \le r \le \beta r_p$) is sufficiently large, the radial displacement at the outer boundaries are zeros; i.e., $u = 0$ at $r = -\beta r_p$ and at $r = \beta r_p$. At the plate edges ($r = -r_p$ and $r = r_p$), the continuity of horizontal displacement and equilibrium of horizontal force are maintained by the following boundary conditions

$$u_{\text{Right}}\big|_{r=-r_p} = u_{\text{Left}}\big|_{r=-r_p} \tag{15a}$$

$$u_{\text{Left}}\big|_{r=r_p} = u_{\text{Right}}\big|_{r=r_p} \tag{15b}$$

$$\left\{C\left(r\frac{du}{dr}+\upsilon_p u\right)+r\frac{du}{dr}\eta_6+\left(\eta_8 u+\eta_1 wr\right)-rN\right\}\Big|_{r=-r_p \ \&\ r=r_p}=0 \tag{15c}$$

To obtain the plate response, differential Eqs. (12(a)) and (14(a)) should be solved along with the corresponding boundary conditions. Note that these two differential equations are coupled because the unknown displacements w and u are present in both the differential equations. Further, it is customary in geotechnical engineering to assume that plates resting on soil have free ends (i.e., the edge of the plate is free to deflect and rotate) because of which the displacements (w and u) are spread beyond the plate edges into the continuum in the radial direction. Therefore, the displacements in the plate and the surface displacements of the soil should be considered together in the solution as these are related. Therefore, Eqs. (12(a)), (12(b)), (14(a)), and (14(b)) should be solved simultaneously to obtain the plate response.

2.7 Differential equations for soil-displacement functions

Considering the variation of the functions ϕ and ψ in Eq. (11) over $0 \le z \le H_{\text{total}}$, the differential equations of $\phi(z)$ and $\psi(z)$ within the i^{th} layer can be obtained as

$$\xi_9\frac{d^2\phi_i}{dz^2}-\xi_8\phi_i=-\left(\xi_3+\xi_5-\xi_7\right)\frac{\partial\psi_i}{\partial z} \tag{16}$$

$$\xi_6\frac{d^2\psi_i}{dz^2}-\left(\xi_2+\xi_1+\xi_4\right)\psi_i=\left(\xi_3+\xi_5-\xi_7\right)\frac{\partial\phi_i}{\partial z} \tag{17}$$

The corresponding boundary conditions are $\phi(0) = 1$, $\phi(H_{\text{total}}) = 0$, and $\phi_i = \phi_{i+1}$ at $z = H_i$, and $\psi(0) = 1$, $\psi(H_{\text{total}}) = 0$, and $\psi_i = \psi_{i+1}$ at $z = H_i$, and these boundary conditions also satisfy Eq. (11). These conditions ensure perfect contact between the plate and the underlying soil, zero displacements at the interface between the soil and underlying rigid layer, and continuity of displacements across the different soil layers.

2.8 Solution of the differential equations

Solution of the plate differential Eqs. (12(a)) and (14(a)) for transverse displacement w, rotation dw/dr, and radial u displacements is obtained by using the displacement-based finite element method. Considering the weak forms of the differential Eqs. (12(a)) and (14(a)) in which the highest derivatives of w and u are d^2w/dx^2 and du/dx, respectively, it is apparent that cubic-Hermitian shape functions are required to interpolate w and dw/dr, and linear-Lagrangian shape functions are required to interpolate u. Thus, over the plate domain $-r_p \le r \le r_p$, two-noded frame elements are used as plate elements such that there are three degrees of

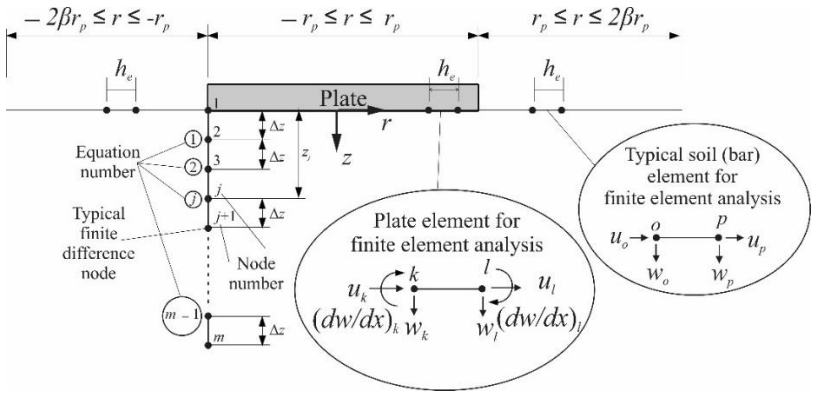

Fig. 2 Finite element and finite difference discretization in r-direction and z-directions

freedom w_k, dw_k/dr and u_k, and w_l, w_l/dr and u_l at the left (k^{th}) and right (l^{th}) nodes, respectively (Fig. 2). Cubic Hermitian shape functions $\{N^w\}^H_{4\times1}$ are used to interpolate w_k, dw_k/dr, w_l and dw_l/dr, and linear Lagrangian shape functions $\{N^u\}^{\mathrm{L}}_{2\times1}$ are used to interpolate u_o and u_p (Fig. 2). These shape functions are given by

$$\{N^w\}^H_{4\times1}=\begin{Bmatrix}N^w_k\\N^{dw/dr}_k\\N^w_l\\N^{dw/dr}_l\end{Bmatrix}=\begin{Bmatrix}1-3\left(\frac{\hat r}{h_e}\right)^2+2\left(\frac{r}{h_e}\right)^3\\-\hat r\left(1-\frac{\hat r}{h_e}\right)^2\\3\left(\frac{\hat r}{h_e}\right)^2-2\left(\frac{r}{h_e}\right)^3\\-\hat r\left[\left(\frac{\hat r}{h_e}\right)^2-\frac{r}{h_e}\right]\end{Bmatrix} \tag{18a}$$

$$\{N^u\}^{\mathrm{L}}_{2\times1}=\begin{Bmatrix}N^u_o\\N^u_p\end{Bmatrix}=\begin{Bmatrix}1-\hat r/h_e\\\hat r/h_e\end{Bmatrix} \tag{18b}$$

where h_e is the length of the element and $\hat r$ is the local radial coordinate within any element with its origin at the left (k^{th}) node.

The use of $\{N^u\}^{\mathrm{L}}_{2\times1}$ and $\{N^w\}^H_{4\times1}$ leads to the following elemental equilibrium equation $[k]^e\{\delta_p\}^e=\{f\}^e$ for any plate element ($[k]^e$, $\{f\}^e$, and $\{\delta_p\}^e$ are the elemental stiffness matrix, elemental force vector, and elemental degrees of freedom vector for the plate element, respectively), given by

$$\begin{Bmatrix}\{\hat k^A_{rz}\}_{4\times4} & \{k^B_{rz}\}_{4\times2}\\ \{\hat k^C_{rz}\}_{2\times4} & \{k^D_{rz}\}_{2\times2}\end{Bmatrix}_{6\times6}\begin{Bmatrix}w_k\\\frac{dw_k}{dr}\\w_l\\\frac{dw_l}{dr}\\u_k\\u_l\end{Bmatrix}_{6\times1}=\begin{Bmatrix}\{f^A_{rz}\}_{4\times1}\\\{f^B_{rz}\}_{2\times1}\end{Bmatrix}_{6\times1} \tag{19}$$

with

$$\begin{aligned}\{\hat k^A_{rz}\}_{4\times4}=\Bigg\{\int_{r_l}^{r_k}\Bigg[&D\frac{d^2N^w}{dr^2}\left(\frac{d^2N^w}{dr^2}\right)^T\\&+\left(\frac{D}{r^2}-2t\right)N^w\left(\frac{d^2N^w}{dr^2}\right)^T\\&-\frac{2D}{r}\frac{dN^w}{dr}\left(\frac{d^2N^w}{dr^2}\right)^T\\&+\left(\frac{D}{r^3}-\frac{2t}{r}\right)N^w\left(\frac{dN^w}{dr}\right)^T+N^wk\left(N^w\right)^T\Bigg]dr\\&+\Bigg[-D\frac{dN^w}{dr}\left(\frac{d^2N^w}{dr^2}\right)^T-\frac{D}{r}N^w\left(\frac{d^2N^w}{dr^2}\right)^T\\&+\left(\frac{D}{r}+2t\right)N^w\left(\frac{dN^w}{dr}\right)^T\Bigg]\Bigg|_{r=r_p}^{r=0}\Bigg\}\end{aligned} \tag{20a}$$

$$\begin{aligned}\{\hat k^B_{rz}\}_{4\times2}=\Bigg\{\int_{r_l}^{r_k}\Bigg[&(\eta_1-\eta_3)N^w\left(\frac{dN^u}{dr}\right)^T\\&+\left(\frac{\eta_1-\eta_3}{r}\right)N^w\left(N^u\right)^T\Bigg]dr+\left[N^w\eta_3\left(N^u\right)^T\right]\Bigg|_{r=r_p}^{r=0}\Bigg\}\end{aligned} \tag{20b}$$

$$\begin{aligned}\{\hat k^C_{rz}\}_{2\times4}=\Bigg\{\int_{r_l}^{r_k}\left[(\eta_3-\eta_1)rN^u\left(\frac{dN^w}{dr}\right)^T\right]dr\\+\left[N^uk\left(N^w\right)^T\right]\Bigg|_{r=r_p}^{r=0}\Bigg\}\end{aligned} \tag{20c}$$

$$\begin{aligned}\{\hat k^D_{rz}\}_{2\times2}=\Bigg\{\int_{r_l}^{r_k}\Bigg[&\left(-\frac{C}{r}-\eta_6\right)N^u\left(\frac{dN^u}{dr}\right)^T\\&+(-C+\eta_8)\frac{dN^u}{dr}\left(\frac{dN^u}{dr}\right)^T\\&+\left(\frac{C}{r^3}+\frac{\eta_6}{r}+\eta_6r\right)N^u\left(N^u\right)^T\Bigg]dr\\&+\Bigg[\left(\frac{\eta_8}{r}+\frac{\upsilon_p}{r}\right)N^u\left(N^u\right)^T\\&+2CN^u\left(\frac{dN^u}{dr}\right)^T\Bigg]\Bigg|_{r=r_p}^{r=0}\Bigg\}\end{aligned} \tag{20d}$$

$$\left\{\hat{f}^{A}_{rz}\right\}_{4\times1}=\left\{\begin{array}{l}\int_{r_l}^{r_k}\left(q(r)N_k^w\right)dr \\ +QN_k^w\big|_{r_p}\quad\int_{r_l}^{r_k}\left(q(r)N_k^{dw/dr}\right)dr+MN_k^{dw/dr}\big|_{r_p} \\ +MN_k^{dw/dr}\big|_{r_p}\int_{r_l}^{r_k}\left(q(r)N_l^w\right)dr \\ +QN_l^w\big|_{r_p}\quad\int_{r_l}^{r_k}\left(q(r)N_l^{dw/dr}\right)dr+MN_l^{dw/dr}\big|_{r_p}\end{array}\right\}^T \tag{20e}$$

$$\left\{\hat{f}^{B}_{rz}\right\}_{2\times1}=\left\{NN_k^u\big|_{r_p}\quad NN_l^u\big|_{r_p}\right\}^T \tag{20f}$$

in which a constant value of distributed load q is assumed within any element (which is a reasonable assumption for small elements), and the matrix indices x and y varies from 1 to 4.

Solution of the differential Eqs. (12(b)) and (14(b)) for soil surface displacements w and u are also obtained using FE analysis. As the highest derivatives of w and u in the weak forms of Eqs. (12(b)) and (14(b)) are dw/dx and du/dx, linear Lagrangian shape functions are required to interpolate both w and u over the elements. Accordingly, two-noded rod (bar) elements with linear Lagrangian interpolation functions described in Eq. (18(b)) are used to discretize the domains $-\beta r_p \le r \le 0$ and $0 \le r \le \beta\, r_p$ (i.e., the domains in radial direction with no plate). This leads to the elemental equilibrium equation $[k]^e\{\delta_s\}^e=\{f\}^e$ for the elements over $-\beta r_p \le r \le 0$ and $0 \le r \le \beta\, r_p$, given by

$$\begin{bmatrix}\left\{\hat{k}^{\searrow}_{rz}\right\}_{2\times2} & \left\{k^{F}_{rz}\right\}_{2\times2}\\ \left\{\hat{k}^{\swarrow}_{rz}\right\}_{2\times2} & \left\{k^{H}_{rz}\right\}_{2\times2}\end{bmatrix}_{4\times4}\begin{Bmatrix}w_o\\w_p\\u_o\\u_p\end{Bmatrix}_{4\times1}=\begin{Bmatrix}0\\0\\0\\0\end{Bmatrix}_{4\times1} \tag{21}$$

$$\left\{\hat{k}^{E}_{rz}\right\}_{2\times2}=\left\{\int_{r_l}^{r_k}\left[2t_s\frac{dN^w}{dr}\left(\frac{dN^w}{dr}\right)^T+k_s rN^w\left(N^w\right)^T-\frac{2t_s}{r}N^w\left(\frac{dN^w}{dr}\right)^T\right]dr\right\} \tag{22a}$$

$$\left\{\hat{k}^{F}_{rz}\right\}_{2\times2}=\left\{\int_{r_l}^{r_k}\left[\frac{(\eta_1-\eta_3)}{r}N^w\left(N^u\right)^T-(\eta_1-\eta_3)N^w\left(\frac{dN^u}{dr}\right)^T+\left[\eta_3N^w\left(N^u\right)^T\right]\Big|_{r=r_p}\right]dr\right\} \tag{22b}$$

$$\left\{\hat{k}^{G}_{rz}\right\}_{2\times2}=\left\{\int_{r_l}^{r_k}\left[(\eta_1-\eta_3)N^u\left(\frac{dN^w}{dr}\right)^T\right]dr+k_sN^u\left(N^w\right)^T\Big|_{r=r_p}\right\} \tag{22c}$$

$$\left\{\hat{k}^{H}_{rz}\right\}_{2\times2}=\int_{r_l}^{r_k}\left[\eta_8\frac{dN^u}{dr}\left(\frac{dN^u}{dr}\right)^T+\frac{\eta_6}{r}N^u\left(\frac{dN^u}{dr}\right)^T+\left(\frac{\eta_6}{r^2}+\eta_7\right)N^u\left(N^u\right)^T\right]dr+\left[(\eta_6-\eta_8)N^u\left(\frac{dN^u}{dr}\right)^T+\frac{\eta_8}{r}N^u\left(N^u\right)^T\right]\Bigg|_{r=r_p} \tag{22d}$$

where $\left\{N^w\right\}^{\mathrm{L}}_{2\times1}=\left\{N^u\right\}^{\mathrm{L}}_{2\times1}$ (Eq. (18b)).

The integrations associated with the elemental stiffness matrix and force vectors described in Eqs. (20) and (22) are performed numerically using Gauss quadrature. The elemental matrices are assembled, and the set of equations are solved to obtain the nodal displacements and rotations.

Differential Eqs. (16) and (17) of ϕ and ψ are interdependent, and thus, must be solved simultaneously. Solutions of the differential Eqs. (16) and (17) of ϕ and ψ are obtained using the finite difference method. The domain in the z direction is discretized, and the central difference scheme is implemented at these points using which Eqs. (16) and (17) can be written as

$$\xi_9\left(\frac{\phi_i^{j+1}-2\phi_i^{j}+\phi_i^{j-1}}{\Delta z^2}\right)-\xi_8\phi_i^{j}=-\left(\xi_3+\xi_5-\xi_7\right)\left(\frac{\psi_i^{j+1}-\psi_i^{j-1}}{2\Delta z}\right) \tag{23}$$

$$\xi_6\left(\frac{\psi_i^{j+1}-2\psi_i^{j}+\psi_i^{j-1}}{\Delta z^2}\right)-\left(\xi_2+\xi_1+\xi_4\right)\psi_i^{j}=\left(\xi_3+\xi_5-\xi_7\right)\left(\frac{\phi_i^{j+1}-\phi_i^{j-1}}{2\Delta z}\right) \tag{24}$$

where j represents the j^{th} node, which is at a vertical distance z_j from the bottom surface of the beam, and Δz is the vertical distance between consecutive nodes. The total number of discretized nodes m should be sufficiently large such that the finite domain in the vertical direction can be adequately modeled (Fig. 2).

Eq. (23) along with the boundary conditions $\phi_i^{(1)}=1$ (at z = 0) and $\phi_i^{(m)}=0$ (at $z = H_{\text{total}}$), is applied to the discretized nodes, yielding the following matrix equation (Eq. (25).

$$\begin{bmatrix}1&0&0&\cdots&&&&&&0\\0&k^{\phi}_{2,2}&k^{\phi}_{2,3}&0&\cdots&&&&&0\\0&k^{\phi}_{3,2}&k^{\phi}_{3,3}&k^{\phi}_{3,4}&0&\cdots&&&&0\\0&0&k^{\phi}_{4,3}&k^{\phi}_{4,4}&k^{\phi}_{4,5}&0&\cdots&&&0\\\vdots&&\ddots&\ddots&\ddots&\ddots&\ddots&&\cdots&\vdots\\0&\cdots&\cdots&0&k^{\phi}_{j,j-1}&k^{\phi}_{j,j}&k^{\phi}_{j,j+1}&0&\cdots&0\\\vdots&&&&\ddots&\ddots&\ddots&\ddots&\ddots&\vdots\\0&\cdots&&&\cdots&0&k^{\phi}_{m-2,m-3}&k^{\phi}_{m-2,m-2}&k^{\phi}_{m-2,m-1}&0\\0&\cdots&&&&\cdots&0&k^{\phi}_{m-1,m-2}&k^{\phi}_{m-1,m-1}&0\\0&\cdots&&&&&\cdots&0&0&1\end{bmatrix}\begin{bmatrix}\phi_i^{(1)}\\\phi_i^{(2)}\\\phi_i^{(3)}\\\phi_i^{(4)}\\\vdots\\\phi_i^{(j)}\\\vdots\\\phi_i^{(m-2)}\\\phi_i^{(m-1)}\\\phi_i^{(m)}\end{bmatrix}=\begin{bmatrix}1\\f^{\phi}_2\\f^{\phi}_3\\f^{\phi}_4\\\vdots\\f^{\phi}_j\\\vdots\\f^{\phi}_{m-2}\\f^{\phi}_{m-1}\\0\end{bmatrix} \tag{25}$$

The non-zero elements of the left-hand side matrix $\left[k^{\phi}\right]_{m\times m}$ in the above equation are given by

$$k_{j,j-1}^{\phi_i} = k_{j,j+1}^{\phi_i} = \frac{\xi_9}{\Delta z^2} \tag{26}$$

$$k_{j,j}^{\phi_i} = \frac{-2\xi_9}{\Delta z^2} - \xi_8 \tag{27}$$

in which the subscript j is valid for nodes 2 to m–1, with the exception that $k_{2,1}^{\phi_i} = 0$ and $k_{m-1,m}^{\phi_i} = 0$ (as evident from Eq. (25)

The elements of the right-hand side vector $\left[f^{\phi_i} \right]_{m\times 1}$ in Eq. (25) are given by

$$f_j^{\phi_i} = -\left(\xi_3 + \xi_5 - \xi_7\right)\left(\frac{\psi_i^{j+1} - \psi_i^{j-1}}{2\Delta z}\right) \tag{28}$$

where j represents nodes 3 through m–2. The elements corresponding to node 2 and m–1 are respectively given by

$$f_2^{\phi_i} = -\frac{\xi_9}{\Delta z^2} - \left(\xi_3 + \xi_5 - \xi_7\right)\left(\frac{\psi_i^3 - 1}{2\Delta z}\right) \tag{29}$$

$$f_{m-1}^{\phi_i} = -\left(\xi_3 + \xi_5 - \xi_7\right)\left(\frac{\psi_i^m}{2\Delta z}\right) \tag{30}$$

Eq. (24) along with the boundary conditions $\psi_i^{(1)} = 1$ (at z = 0) and $\psi_i^{(m)} = 0$ (at $z = H_{\text{total}}$), is applied to the discretized nodes, and a matrix equation (similar to Eq. (25)) for ψ_i can be formed for the discretized nodes as

$$\left[k^{\psi_i}\right]\{\psi_i\} = \left\{f^{\psi_i}\right\} \tag{31}$$

The non-zero elements of the left-hand side matrix $\left[k^{\psi_i}\right]_{m\times m}$ in the above equation are given by

$$k_{j,j-1}^{\psi_i} = k_{j,j+1}^{\psi_i} = \frac{\xi_6}{\Delta z^2} \tag{32}$$

$$k_{j,j}^{\psi_i} = \frac{-2\xi_6}{\Delta z^2} - \left(\xi_2 + \xi_1 + \xi_4\right) \tag{33}$$

in which the subscript j is valid for nodes 2 to m–1, with the exception that $k_{2,1}^{\psi_i} = 0$ and $k_{m-1,m}^{\psi_i} = 0$.

The elements of the right-hand side vector $\left[f^{\psi_i} \right]_{m\times 1}$ in Eq. (31) are given by

$$f_j^{\psi_i} = \left(\xi_3 + \xi_5 - \xi_7\right)\left(\frac{\phi_i^{j+1} - \phi_i^{j-1}}{2\Delta z}\right) \tag{34}$$

where j represents nodes 3 through m–2. The elements corresponding to node 2 and m–1 are respectively given by

$$f_2^{\phi_i} = -\frac{\xi_6}{\Delta z^2} + \left(\xi_3 + \xi_5 - \xi_7\right)\left(\frac{\phi_i^{(3)} - 1}{2\Delta z}\right) \tag{35}$$

$$f_{m-1}^{\phi_i} = \left(\xi_3 + \xi_5 - \xi_7\right)\left(\frac{\phi_i^m}{2\Delta z}\right) \tag{36}$$

As the right-hand side vectors $\left[f^{\phi_i} \right]_{m\times 1}$ and $\left[f^{\psi_i} \right]_{m\times 1}$ contain the unknowns ϕ_i and ψ_i, iterations are necessary to obtain their values. An initial estimate of ϕ_i^j is made and given as input to $\left[f^{\psi_i} \right]_{m\times 1}$, and ψ_i^j is determined by solving Eq. (31). The ψ_i^j values are then given as input to $\left[f^{\phi_i} \right]_{m\times 1}$, to obtain ϕ_i^j by solving Eq. (25). The newly obtained values of ϕ_i^j are again used to obtain new values of ψ_i^j, and the iterations are continued until convergence is reached.

2.9 Iterative solution algorithm

The soil parameters η_α (α = 1-8) must be known in order to solve the system of equations for w and u, and these coefficients depend upon ϕ and ψ. At the same time, the parameters ξ_μ (μ = 1-9) must be known in order to obtain ϕ and ψ, and these parameters depend upon w and u. Therefore, equations of w, u, ψ and ϕ are coupled and are solved simultaneously following an iterative scheme.

Initial guesses for the parameters ξ_μ are made and the equations of ϕ and ψ are solved. The obtained values of ϕ and ψ are used to calculate the parameters η_α. The calculated η_α values are then used to solve for the displacements w and u, which are then used to calculate a new set of values of the parameters ξ_μ. These newly calculated set of ξ_μs are compared with the corresponding assumed ξ_μ values and if the difference is greater than a tolerable limit, then the calculations described above are repeated with the calculated ξ_μ as the new guess. The iterative calculations are continued until the assumed and calculated ξ_μ values fall within a tolerable limit. The prescribed tolerance limit set for the iterations is 10^{-5}. A detailed solution algorithm is given in Fig. 3.

3. Results

The accuracy of the analysis is verified with the help of five example problems. The plate-soil responses obtained for the example problems using the present analysis are compared with those obtained from equivalent axisymmetric FE analysis performed using Plaxis 2D and with those obtained by other researchers as reported in the literature. In Plaxis, the plate is modeled using one dimensional (1D) plate elements, and the foundation is modeled using axisymmetric 6-noded triangular elements. Plaxis automatically generates an interface between the plate and foundation to ensure that full contact is maintained during loading. Appropriate boundary conditions are prescribed at the continuum boundaries of the axisymmetric FE model — all components of displacement are assumed to be zero along the bottom (horizontal) boundary and the horizontal component of displacement is assumed to be zero

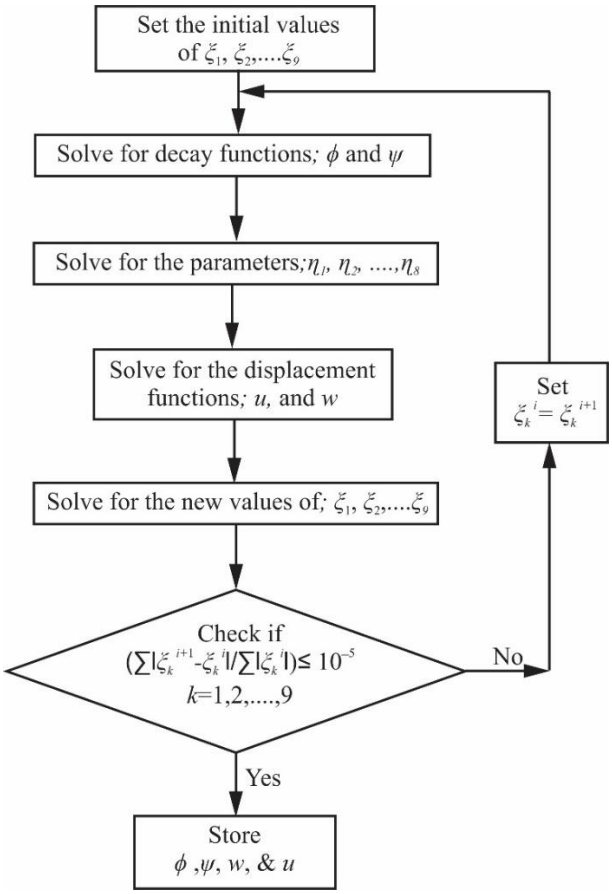

Fig. 3 Solution algorithm

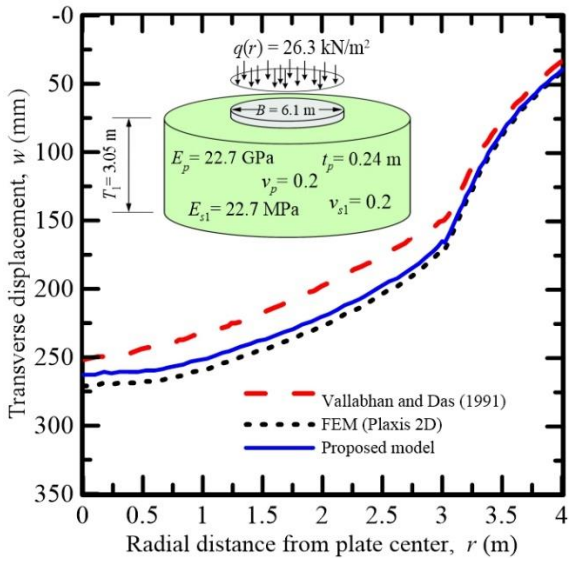

Fig. 4 Verification example 1: transverse displacement of a circular plate on a single-layer soil deposit

along the outer vertical boundary of the domain. Boundary conditions are prescribed at the edge of the plate to ensure that the edge is free to deflect and rotate (for plates with free ends, which is what is assumed in this study).

As the first verification problem, a circular plate with free edges and with r_p = 3.05 m, t_p = 0.24 m, E_p = 22.7 GPa, and υ_p = 0.2 is considered. The plate rests on a single layer, homogeneous soil deposit of thickness H_{total} = 3.05 m with E_s = 22.7 MPa and υ_s = 0.2. The plate is subjected to a uniformly distributed load of 26.3 kN/m^2 acting over the entire area of the plate. This problem was analyzed by Vallabhan and Das (1991) considering only non-zero vertical displacements in the soil. The details of the properties of the plate-foundation system are given in Fig. 4.

Table 1 Computational efficiency of the present analysis

Figure	CPU time (sec)		Computational efficiency (%) (FE-PS)/PS
	Present solution (PS)	2-D FE analysis (FE)	
4	4	7	75
5	3.8	6.2	63
6	5.8	11.1	91
7	7.4	13.2	78
8	8.5	15.7	84

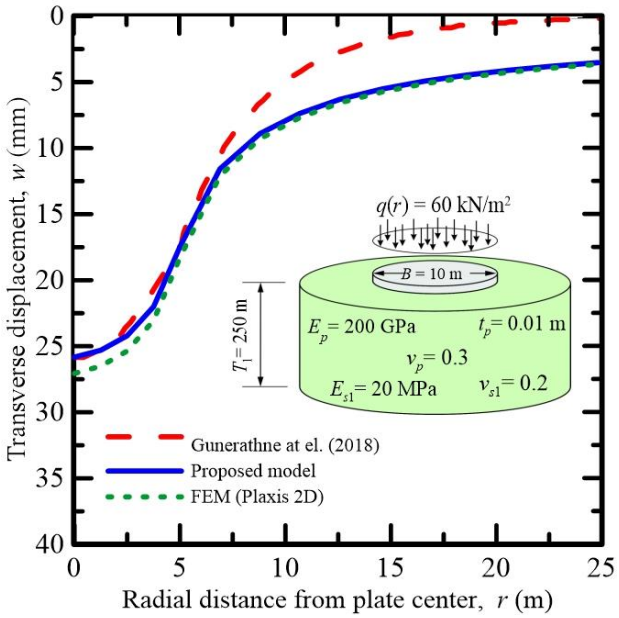

Fig. 5 Verification example 2: transverse displacement of a circular plate on a single-layer soil deposit

Fig. 4 also shows the deflected shape (settlement) $w(r)$ of the plate obtained from the present analysis, from the FE analysis using Plaxis 2D, and by Vallabhan and Das (1991). The present analysis matches the FE results quite well and the match between the results of the present analysis and FE analysis is better than that between the results of Vallabhan and Das (1991) and the FE analysis.

For the second example, a 10 m diameter circular steel tank-foundation with free edges and with t_p = 0.01 m, E_p = 200 GPa, and υ_p = 0.3, and resting on a single-layer soil deposit of thickness H_{total} = 250 m, E_s = 20 MPa and υ_s = 0.2 is considered. The plate is subjected to a uniformly distributed load of 60 kN/m^2 acting over the entire area of the plate. This problem was analyzed by Gunerathne *et al.* (2018) considering only non-zero vertical displacements in the soil. The details of the properties of the plate-foundation system are given in Fig. 5. Fig. 5 also shows the deflected shape (settlement) $w(r)$ of the plate obtained from the present analysis, from the FE analysis using Plaxis 2D, and from Gunerathne *et al.* (2018). The present analysis matches the FE results quite well and the match between the results of the present analysis and FE analysis is better than that between the results of Gunerathne *et al.* (2018) and FE analysis.

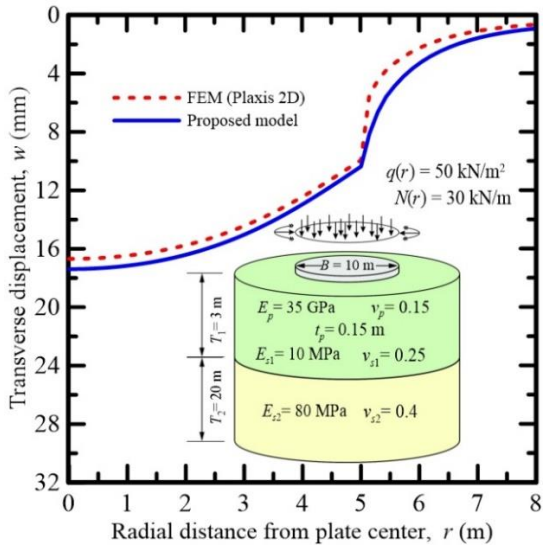

Fig. 6 Verification example 3: transverse displacement of a circular plate on a two-layer soil deposit

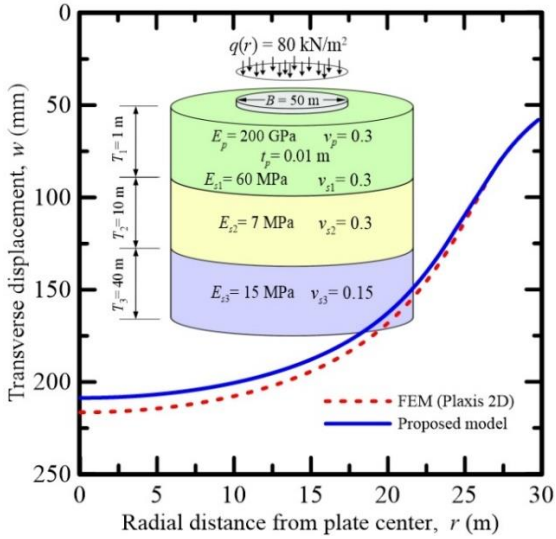

Fig. 7 Verification example 4: transverse displacement of a circular plate on a three-layer soil deposit

For the third, fourth, and fifth verification examples, three circular tank-foundations with free edges are assumed to rest on two, three, and four-layered soil deposits, respectively. The plates are subjected to a combination of uniformly distributed loads acting over the areas of the plates and radial compressive loads acting along the perimeter of the plates. The details of the properties of the plate-foundation systems are given in Figs. 6-8, respectively. Comparisons of the transverse displacements (settlement) $w(r)$ obtained from the present analysis and the axisymmetric FE analysis are also shown in Figs. 6-8, respectively. It is evident from the figures that the responses obtained from the present analysis and axisymmetric FE analysis are in good agreement, with the maximum difference being 7.5%.

The analyses were performed in a computer with Intel core i7-3.6 GHZ processor and 16 GB DDR3 RAM. The computational times required for the problems described in

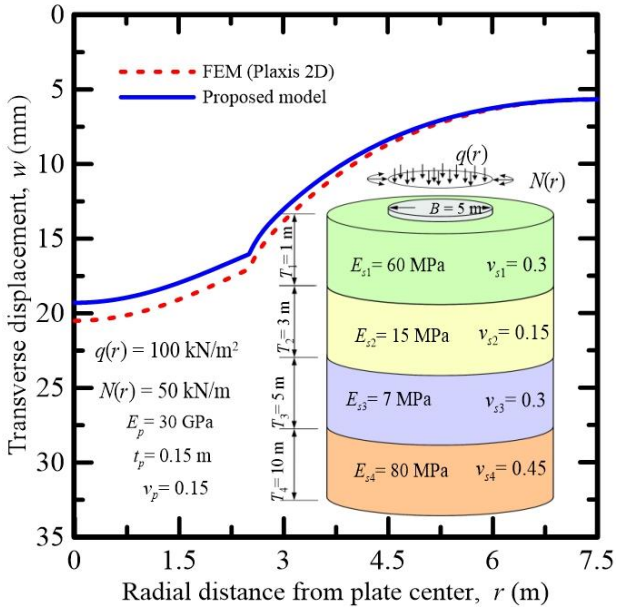

Fig. 8 Verification example 5: transverse displacement of a circular plate on a four-layer soil deposit

Figs. 4-8 are given in Table 1. The table shows that the present method takes approximately half the time taken by equivalent 2D FE analysis to solve a problem. Because the developed analysis framework involves the solution of four one-dimensional differential equations (as opposed to two-dimensional equations), solution using the present method is obtained faster than equivalent 2D FE analysis.

4. Conclusions

A framework for analysis of thin circular plates resting on multi-layered elastic soil deposits and subjected to axisymmetric vertical and horizontal loads, and moments is developed. The Kirchhoff plate theory is used to model the plate and the small strain hyper-elastic theory is used to model the soil. The displacements in the soil are assumed to be products of separable variables. The potential energies of the plate, multi-layered soil, and the externally applied loads are summed to obtain the total potential energy of the plate-soil system, which is then minimized to obtain the differential equations governing the displacements of the plate and soil. The differential equations are solved using finite element and finite difference methods following an iterative algorithm.

The accuracy of the analysis is verified by comparisons with equivalent two-dimensional finite element analysis performed using Plaxis. The verification study also includes comparisons of results obtained by other researchers. The analysis can produce accurate predictions of maximum and differential settlements, and angular distortions of plates resting on multi-layered soil. The analysis produces results faster than those from equivalent 2D FE analysis. The newly developed analysis can be used in design if the elastic properties of the plate and soil are accurately estimated.

5. Data availability statement

Some or all data, models, or code generated or used during the study are available from the corresponding author by request as detailed below:

- A version of the code used to generate some of the results in this paper.

References

Ahlvin, R.G. and Ulery, H.H. (1962), "Tabulated values for determining the complete pattern of stresses, strains, and deflections beneath a uniform circular load on a homogeneous half space", *Highway Res. Board Bull*., 342.

Bell, R.A. and Iwakiri, J. (1980), "Settlement comparison used in tank-failure study", *J. Geotech. Eng. Div. - ASCE*, **106**(2), 153-169. https://doi.org/10.1061/AJGEB6.0000919.

Bowles, L.E. (1996), Foundation analysis and design. McGraw-hill.

Booker, J.R. and Small, J.C. (1983), "The analysis of liquid storage tanks on deep elastic foundations", *Int. J. Numer. Anal. Met*., **7**(2), 187-207. https://doi.org/10.1002/nag.1610070205.

Brown, P.T. (1969), "Numerical analyses of uniformly loaded circular rafts on elastic layers of finite depth", *Geotechnique*, **19**(2), 301-306. https://doi.org/10.1680/geot.1969.19.2.301.

Buczkowski, R. and Torbacki, W. (2001), "Finite element modelling of thick plates on two-parameter elastic foundation", *Int. J. Numer. Anal. Met*., **25**(14), 1409-1427. https://doi.org/10.1002/nag.187.

Chandrasekaran, K. and Kunukkasseril, V.X. (1976), "Forced axisymmetric response of circular plates", *J. Sound Vib*., **44**(3), 407-417. https://doi.org/10.1016/0022-460X(76)90511-3.

D'Orazio, T.B. and Duncan, J.M. (1987), "Differential settlements in steel tanks", *J. Geotech. Eng*., **113**(9), 967-983. https://doi.org/10.1061/(ASCE)0733-9410(1987)113:9(967).

Filonenko-Borodich, M.M. (1945), "A very simple model of an elastic foundation capable of spreading the load", *Sb. Tr. Mosk. Elektro. Inst, Inzh. Trans*, 53.

Galvis, F.A. and Smith-Pardo, J.P. (2020), "Axial load biaxial moment interaction (PMM) diagrams for shallow foundations: Design aids, experimental verification, and examples", *Eng. Struct.*, **213**, 110582. https://doi.org/10.1016/j.engstruct.2020.110582.

Gerrard, C.M. and Harrison, W.J. (1970), Stresses and displacements in a loaded orthorhombic half space.

Ghali, A. (2003), Circular storage tanks and silos, CRC Press.

Girija Vallabhan, C.V. and Das, Y.C. (1991), "Analysis of circular tank foundations", *J. Eng. Mech*., **117**(4), 789-797. https://doi.org/10.1061/(ASCE)0733-9399(1991)117:4(789).

Gunerathne, S., Seo, H., Lawson, W.D. and Jayawickrama, P.W. (2018), "Analysis of edge-to-center settlement ratio for circular storage tank foundation on elastic soil", *Comput. Geotech*., **102**, 136-147. https://doi.org/10.1016/j.compgeo.2018.05.008.

Gunerathne, S., Seo, H., Lawson, W.D. and Jayawickrama, P.W. (2019), "Variational approach for settlement analysis of circular plate on multilayered soil", *Appl. Math. Model*., **70**, 152-170. https://doi.org/10.1016/j.apm.2019.01.009.

Hetenyi, M. (1946), Beams on Elastic Foundation. The University of Michigan Press, Ann Arbor, sect. 56.

Hemsley, J.A. and WINKLER. (1987), "Elastic solutions for axisymmetrically loaded circular raft with free or clamped edges founded on Winkler springs or a half-space", *P. I. Civil Eng.*, **83**(1), 61-90. https://doi.org/10.1680/iicep.1987.342.

Jones, G. (1997), Analysis of beams on elastic foundations: using finite difference theory. Thomas Telford.

Komlev, A.A. and Makeev, S.A. (2018), "The calculation of rectangular plates on elastic foundation the finite difference method', *J. Physics: Conference Series*, **944**(1), 012056). https://doi.org/10.1088/1742-6596/944/1/012056.

Kukreti, A.R. and Siddiqi, Z.A. (1997), "Analysis of fluid storage tanks including foundation-superstructure interaction using differential quadrature method", *Appl. Math. Model*., **21**(4), 193-205. https://doi.org/10.1016/S0307-904X(97)00007-3.

Li, R., Zhong, Y. and Li, M. (2013), "Analytic bending solutions of free rectangular thin plates resting on elastic foundations by a new symplectic superposition method", *P. Roy. Soc. A: Math. Phy.*, **469**(2153), 20120681. https://doi.org/10.1098/rspa.2012.0681.

Marr, W.A., Ramos, J.A. and Lambe, T.W. (1982), "Criteria for settlement of tanks", *J. Geotech. Eng. Div*., **108**(8), 1017-1039. https://doi.org/10.1061/AJGEB6.0001326.

Mahmood, I.U. (1984), "Finite element analysis of cylindrical tank foundations resting on isotropic soil medium including soil-structure interaction", Doctoral dissertation; University of Oklahoma.

Melerski, E.S. (1991), "Simple elastic analysis of axisymmetric cylindrical storage tanks", *J. Structu. Eng*., **117**(11), 3239-3260.

Pasternak, P.L. (1954), On a new method of analysis of an elastic foundation by means of two foundation constants, Gosudarstvennoe Izdatelstvo Literaturi po Stroitelstvu i Arkhitekture, Moscow.

Pavlovic, M.N. (2001), "Design analysis of beams, circular plates and cylindrical tanks on elastic foundations-Edmund S. Melerski, AA Balkema, Rotterdam, 1995, xxii+ 284 pp", *Eng. Struct*., **5**(23), 576-577.

Reddy, J.N. (2006), Theory and analysis of elastic plates and shells, CRC press.

Remadna, M.S., Benmebarek, S. and Benmebarek, N. (2017), "Numerical evaluation of the bearing capacity factor N'c of circular and ring footings", *Geomech. Geoeng*., **12**(1), 1-13. https://doi.org/10.1080/17486025.2016.1153729.

Rosenberg, P. and Journeaux, N.L. (1982), "Settlement limitations for cylindrical steel storage tanks", *Can. Geotech. J*., **19**(3), 232-238. https://doi.org/10.1139/t82-030.

Salgado, R. (2008), The engineering of foundations, (Vol. 888). New York: McGraw-Hill.

Straughan, W.T. (1990), "Analysis of plates on elastic foundations", Doctoral dissertation; Texas Tech University).

Timoshenko, S.P. and Woinowsky-Krieger, S. (1959), Theory of plates and shells, McGraw-hill.

Turhan, A. (1992), "A consistent Vlasov model for analysis of plates on elastic foundations using the finite element method", Doctoral dissertation; Texas Tech University.

Useche-Infante, D., Aiassa Martinez, G., Arrúa, P. and Eberhardt, M. (2022), "Experimental study of behaviour of circular footing on geogrid-reinforced sand", *Geomech. Geoeng*., **17**(1), 45-63. https://doi.org/10.1080/17486025.2019.1683621.

Useche-Infante, D., Aiassa Martínez, G., Arrúa, P. and Eberhardt, M. (2021), "Scale effect on the behavior of circular footing on geogrid-reinforced sand using numerical analysis", *Geomech. Geoeng*., **18**(1), 1-14. https://doi.org/10.1080/17486025.2021.2007301.

Utku, M., Çıtıpıtıoğlu, E. and Inceleme, I. (2000), "Circular plates on elastic foundations modelled with annular plates", *Comput. Struct*., **78**(1-3), 365-374. https://doi.org/10.1016/S0045-7949(00)00063-8.

Vallabhan, C.V. and Das, Y.C. (1989), "Beams on elastic foundations: a new approach", In Foundation Engineering: Current Principles and Practices, 613-624.

Vallabhan, C.V. and Das, Y.C. (1991), "Analysis of circular tank foundations", *J. Eng. Mech*., **117**(4), 789-797. https://doi.org/10.1061/(ASCE)0733-9399(1991)117:4(789).

Vlasov, V.Z. and Leontiev, N.N. (1966), "Beams, plates, and shells on elastic foundations", translated from Russian by Israel program for scientific translations, NIST No. N67-14238.

Winkler, E. (1867), Theory of elasticity and strength. Dominicus Prague.

Worku, A. and Habte, B. (2022), "Analytical formulation and finite-element implementation technique of a rigorous two-parameter foundation model to beams on elastic foundations", *Geomech. Geoeng.*, **17**(2), 547-560. https://doi.org/10.1080/17486025.2020.1827162.

Yang, T.Y. (1972), "A finite element analysis of plates on a two parameter foundation model", *Comput. Struct*., **2**(4), 593-614. https://doi.org/10.1016/0045-7949(72)90011-9.

IC

Notations

Nomenclature	Description
B	Diameter of circular plate
r_p	Radius of circular plate
t_p	Plate depth (thickness)
E_p	Young's modulus of plate
υ_p	Poisson's ratio of plate
C	Extensional rigidity of plate
D	Flexural rigidity of plate
n	Number of layers of the multi-layered continuum (soil)
T_i	Thickness of the soil layer i^{th} within the continuum
H_{total}	The total thickness of the n layers
H_i	Vertical elevation within the soil continuum measured form the top
(r-θ-z)	A right-handed cylindrical coordinate system (r-θ-z)
Q	Transverse (vertical) line load
$q(r)$	Distributed transverse (vertical) load
M	Line moment load
N	Radial (horizontal) load
β	Dimensionless factor
u_r	The radial (horizontal) soil displacement
u_z	The vertical soil displacement u_z
$w(r)$	The vertical displacement at the top surface of the continuum
$u(r)$	The radial (horizontal) displacement at the top surface of the continuum
$\phi(z)$	Dimensionless displacement function varying with depth
$\psi(z)$	Dimensionless displacement function varying with depth
ε_{ij}	The strain tensor at any point in the continuum (soil)
σ_{ij}	The stress tensor at any point in the continuum (soil)
$\bar{E}_{si}$	The constrained modulus of the i^{th} soil layer
$U_{D\text{-soil}}$	The strain energy density over the entire soil volume participating in the deformation
G_{si}	The shear modulus of the i^{th} soil layer
E_{si}	The elastic modulus of the i^{th} soil layer
υ_{si}	The Poisson's ratio of the i^{th} soil layer
Π_{soil}	The total potential energy of the soil continuum
Ω_{soil}	The entire soil volume participating in the deformation
Π_{plate}	The potential energy of a circular plate in polar coordinates, including both extensional and transverse displacements
$U_{D\text{-plate}}$	The strain energy density of the plate considering both extensional and transverse displacements
Ω_{plate}	The plate volume participating in the deformation
Π_{system}	The total potential energies of the plate-soil system
δ	The variational operator
Π_{load}	The external work done by the non-conservative forces acting on the system
∇	The Laplacian differential operator
η_{1-8}	Integral parameters
ξ_{1-9}	Integral parameters
$\left\{N^w\right\}^H_{4\times1}$	Cubic Hermitian shape functions
$\left\{N^u\right\}^{\text{L}}_{2\times1}$	Linear Lagrangian shape functions
d/dr	First spatial derivative in the radial direction
d^2/dr^2	Second spatial derivative in the radial direction
d/dz	First spatial derivative in the vertical direction
d^2/dz^2	Second spatial derivative in the vertical direction
h_e	The length of the finite element
$\hat{r}$	The local radial coordinate of the finite element
$[k]^e$	The elemental stiffness matrix of the soil-plate system
$\{f\}^e$	The elemental force vector of the soil-plate system
$\{\delta\}^e$	The elemental degrees of freedom for the soil-plate system
Δz	The vertical distance between two consecutive nodes
m	The total number of discretized nodes in z-direction